Nuclear Inst. and Methods in Physics Research, A 871 (2017) 142–147

Contents lists available at ScienceDirect

Nuclear Inst. and Methods in Physics Research, A

journal homepage: www.elsevier.com/locate/nima

Thin CVD diamond film detector for slow neutrons with buried graphitic electrode

A.P. Bolshakov [a,b,c,*], K.N. Zyablyuk [d], V.A. Kolyubin [d], V.A. Dravin [e], R.A. Khmelnitskii [b,e,f,g], P.G. Nedosekin [d], V.N. Pashentsev [c,d], E.M. Tyurin [c], V.G. Ralchenko [a,b,c]

[a] Harbin Institute of Technology, 92 Xidazhi Str., 150001 Harbin, PR China
[b] General Physics Institute, Russian Academy of Sciences, Vavilova Str. 38, 119991 Moscow, Russia
[c] National Research Nuclear University "MEPhI", Kashirskoye sh. 31, 115409 Moscow, Russia
[d] UralAlmazInvest Industrial Technological Center, Ivana Franko Str. 4, 121108 Moscow, Russia
[e] Lebedev Physical Institute, Russian Academy of Sciences, Leninskii Prosp. 53, 119991 Moscow, Russia
[f] Institute of Radio Engineering and Electronics, Russian Academy of Sciences, Fryazino, Moscow Region, 141190, Russia
[g] Troitsk Institute for Innovation and Fusion Research, Pushkovykh Str. 12, Troitsk, Moscow Region, 142190 Russia

ARTICLE INFO

Keywords:
Diamond film
Neutron detector
Ion implantation
Graphite contacts
α-particles

ABSTRACT

We fabricated neutron detectors based on thin epitaxial CVD diamond films grown on single crystal diamond substrates, with a buried graphitic electrode produced by ion implantation and annealing. The spectra of 5.5 MeV alpha particles were measured with ≈3.5% energy resolution, and, based on the features of those spectra, a precise assessment of the film thickness was able achieved. A 10 μm thick detector was tested for ^{252}Cf neutron and γ-radiation source, using ^{10}B and ^{6}Li isotopes as converters. Due to the small film thickness the contribution from the γ-quanta background to the spectra was restricted by energies below 200 keV, and could be easily discriminated from the neutron related signals. The performance of the detectors was tested for 5.5 MeV α-particles at fluences up to 10^{9} cm^{-2}, and no detrimental polarization effect was observed for the best sample.

1. Introduction

Diamond detectors of ionizing radiation have certain advantageous, such as high radiation hardness, performance at high elevated temperatures, and fast response, in comparison with common semiconducting devices. The diamond detectors are of interest for neutron flux control in nuclear reactors [1,2], dose measurement in neutron-capture medical therapy [3], thermonuclear plasma research [4–17]. Commonly, the neutron detector contains a converter, i.e. a material with isotopes having a high cross-section of interaction with slow neutrons, to generate high energy charged particles, to be eventually detected. The compounds with stable isotopes of boron ^{10}B and lithium ^{6}Li are often used in the converters.

Of particular interest are experiments on fusion reactors (tokamaks), where diamond detectors measure simultaneously the total neutron flux and fast 14 MeV neutrons generated in deuterium–tritium plasma [4]. The fast neutrons are detected owing to $^{12}C(n,\alpha)^{9}Be$ reaction within the bulk of diamond crystal, therefore the detection efficiency is proportional to the crystal thickness. However, with increase of the detector thickness the unwanted sensitivity to γ-radiation, more specifically, to Compton electrons formed as a result of γ quanta interaction with the diamond and surrounded materials, also increases. While the *n*-detectors performance is tested, as a rule, with neutron generators, which possess only a weak X-ray background, many other neutron sources, such as heavy fission nuclei, have a significant level of concomitant γ-radiation. Particularly, recent experiments with 0.5 mm thick diamond detector with ^{10}B converter using ^{252}Cf neutron source [18] demonstrated that the major part of the detector signal was induced by the γ-radiation. As the Compton electrons exhibit a small linear energy loss and a long free path in diamond, the decrease of diamond thickness can be an effective means to reduce the γ-background signal [19].

Thin-film diamond detectors are widely investigated in the literature [1,3–7,17]. Typically this type of detector has a boron-doped diamond layer produced by chemical vapor deposition (CVD) as backing contact and the intrinsic diamond sensitive layer epitaxially grown on it. The boron doped substrate, grown either by CVD or by high-pressure high temperature (HPHT) technique, can have defects induced by the boron doping (and even a change in lattice parameter in case of high

* Corresponding author at: General Physics Institute, Russian Academy of Sciences, Vavilova Str. 38, 119991 Moscow, Russia.
E-mail address: bolshak@ran.gpi.ru (A.P. Bolshakov).

http://dx.doi.org/10.1016/j.nima.2017.07.058
Received 8 June 2017; Received in revised form 24 July 2017; Accepted 27 July 2017
Available online 5 August 2017
0168-9002/

doping level), which result in defects appearance in the top epitaxially deposited intrinsic sensitive diamond film. It might be a reason why the quality of the sensitive layer is usually worse, than that of free-standing CVD plates, directly grown on undoped HPHT crystals. While the latter readily reach 0.4% energy resolution for 5.5 MeV α-particles, the resolution of ~20 μm-thick detectors with boron-doping backing contact is reported to be not higher than 1%–2% [4,6,7]. The best resolution 0.5% was reported in [4], but only for a thick 100 μm sample. What is more important, defects in the sensitive layer can reduce the detector performance when working under high radiation fluxes and doses due to polarization effect, observed even in the high-quality free-standing CVD crystal plates [20].

A buried graphitic layer inside the intrinsic diamond as the backing contact is considered here an alternative option to the boron-doped contact for the thin-film diamond detectors. Recently [21] we fabricated a thin (~9 μm) diamond film detector with the buried graphitic layer, and its preliminary test demonstrated the realistic spectrum from ^{252}Cf source with only small γ-background contribution. In the present work we further extended the study of this type of thin film detector. The detectors on three diamond films epitaxially grown on different sorts of single crystal (SC) substrates, have been fabricated and tested. The spectra of α-sources with 5.5 MeV energy have been obtained, and used to estimate the diamond film thickness with SRIM program [22]. The stability of the device performance upon prolonged α-particle irradiation was examined, and a polarization effect have been revealed, different for the samples compared. One of the detectors, with the largest crystal area, was used to measure the signal spectrum from ^{252}Cf neutron source. The contribution of γ-radiation to the signal was deduced from comparison of the detector performance with and without ^{10}B and ^{6}Li converters. These results are important for appropriate choice of the minimum signal detection threshold in presence of high γ-background.

2. Experimental

Three detectors were fabricated by growing CVD diamond films on synthetic SC diamond substrates, all with (100) orientation of largest face. The sample H1 was deposited on a commercial Ib type synthetic high pressure-high temperature (HPHT) diamond substrate with dimensions $5.0 \times 4.5 \times 0.5$ mm^3, and with a nitrogen concentration of the order of 100 ppm. Two other devices were formed on the films deposited on $2.5 \times 2.5 \times 0.5$ mm^3 low-nitrogen type IIa HPHT substrate from "NDT LLC" [23] (sample H2) and on IIa type CVD diamond substrate $5.6 \times 5.6 \times 0.4$ mm^3 from "SoniTools" [24] (sample ST). The sample preparation was similar to that described in [21]. First, an epitaxial film with thickness of ~3 μm was grown in a microwave plasma CVD system ARDIS-100 [25], keeping the following process parameters: $CH_4(3\%)/H_2$ gas mixture, total flow rate of 500 sccm, pressure 130 Torr, microwave power of 3.0 kW, substrate temperature ≈980 °C, deposition time of 1 h. Second, He^+ ion implantation in the diamond film (energy of 350 keV, dose of 4×10^{16} cm^{-2}) was performed at room temperature to form a buried damaged layer in the first CVD diamond layer, followed by annealing in vacuum at 1500 °C for 1 h to graphitize this amorphous material and obtain a high electrical conductivity. The thin graphitic layer was located at the depth of about 700 nm (according to TRIM calculation the projected range for α-particles is 752 ± 44 nm), well within the CVD film. The estimated thickness of the graphitic layer for the implantation conditions used was about 60 nm, as deduced from optical spectroscopy measurements in a previous work [26].

The ion implantation forms defects (vacancies and interstitial carbon atoms) along the path of impinging He^+ ion. It is assumed that the annealing in vacuum at 1500 °C for 1 h results in two effects. First, a thin buried layer of the disordered material, where the concentration of vacancies exceeds some critical value, is converted to graphite. Second, the defected diamond cap above the graphical layer is annealed completely (vacancies annealed out at temperatures above 800 °C), almost fully restoring the structure [27]. The annealing procedure is absolutely necessary for preserving good quality of diamond on the graphitic contact.

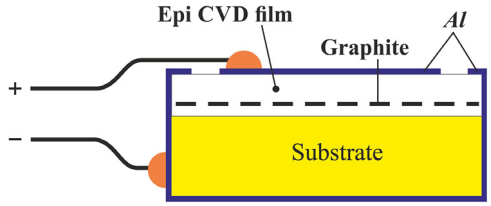

Fig. 1. Schematic view of the detector with the top CVD diamond film, buried graphitic layer and top *Al* electrode.

Then, the epitaxial growth of CVD diamond layer was repeated at the same process parameters, but for a longer time of 3 h, to obtain the top film thickness of about 10 μm. Because of the deposition temperature fluctuations and/or drift, the growth rate was not exactly the same in different deposition runs, the final thickness could vary by ~20% as discussed further in Section 3.1. The film surfaces were not polished, they exhibited growth features (growth steps) with height of 10 to 80 nm, as observed with an optical profilometer ZYGO NewView500. The surface roughness for the samples varied from 24 to 80 nm, while peak-to-valley height ranged from 200 to 700 nm. The CVD diamond layer, due to its high purity, served as the sensitive element of the detector. Finally, all four edges of the sample were mechanically polished to get an access to the buried graphitic contact.

The diamond plate was then metalized with ~100 nm *Al* film on all sides by magnetron sputtering in Ar gas at pressure of 10 mTorr. Using a photolithography the top electrode was formed on the epifilm surface, with 0.4 mm open gap along the edges for isolation. The design of the detector is shown schematically in Fig. 1.

The area of the top *Al* contact was 3.3×3.3 mm^2, 1.6×1.6 mm^2 and 3.7×3.7 mm^2 for the samples H1, H2 and ST, respectively. The wires were fixed to the electrodes with a silver paste. The dark (leakage) current at bias voltage of −25 to + 25 V was measured with the Keithley 6485 picoamperemeter. For the samples ST and H2 the dark current was below the noise level of ~20 pA for all bias range, as estimated by removing the samples from the measurement circuit. However, for the H1 sample a diode behavior was observed at the voltage above −7 V on the top contact. The leakage current above this bias value was rather unstable and demonstrated hysteresis behavior, so its *I-V* characteristics is not shown here. However the current returned below the noise level when the voltage was rising, therefore no breakdown occurred for H1. Attempts to use negative bias for ST and H2 samples were discarded, since the spectra had high noise signal level in this case. This can indicate an effect of hole injection from the graphite contact, similar to what was reported for diamond detectors with boron-doped contact layer [5]. Therefore, all measurements of the spectra were performed at positive bias voltage on the top electrode.

3. Results

3.1. Alpha particles spectra

The ^{238}Pu source emitting alphas with energies 5.499 MeV (71%) and 5.456 MeV (29%) was used for the α-spectra measurements. To avoid the edge effects the source was positioned above a diaphragm of 1.5 mm diameter placed in the center of the detector crystal. The distance between the α-source and the top surface of the detector was 1 mm. The detector was mounted in a metal enclosure, with output cable connected to a charge-sensitive amplifier (the same as described in [28]) and SBS-77 multichannel analyzer (MCA) with build-in bias supply. The measurements were performed in vacuum at + 20 V bias, each spectrum being recorded for 10 min at fixed MCA settings.

The spectra obtained with the three detectors exhibit alpha-peak with width (FWHM) of 3%–4% as displayed in Fig. 2. This width is limited by the performance of the amplifier used in the experiment, rather than by CVD layer quality. The amplifier noise was estimated using a test pulse generator, the pulse amplitude was adjusted equal to that of the signal from the 5.5 MeV α-particle in diamond. The test pulse width measured with the MCA was ≈2%, corresponding to 100 keV energy deposition in diamond. For comparison purpose we also measured the response of a detector we fabricated on a 0.5 mm thick commercial electronic grade SC diamond (Element Six), and obtained the similar energy resolution of 3% for the alpha-peak on 650 channel.

According to SRIM calculation [22] the projected range of an alpha-particle in diamond is 13.6 μm, that exceeds the CVD diamond film thickness (~10 μm) above the buried contact. Therefore, the particles, impinging on the detector surface almost vertically, traverse through the film and deposit only a part of their energy in the sensitive CVD layer (above graphite electrode). This explains the origin of a shoulder present in the spectra for samples H1 and ST (see Fig. 2(a), (c)). At the same time the particles escaping the diaphragm along tilted directions leave all their energy in the sensitive layer and form the sharp peak on Fig. 2(a)–(c). To check this assumption the experiment was repeated with the 1.5 mm diameter diaphragm but with thickness increased to 8 mm. This diaphragm collimated the incident particles by passing only those directed within a narrow cone of about 10° with respect to the vertical. The counting rate in this case decreased down to 0.2 c^{-1}, so we had to increase the spectrum recording time up to 30 min.

The spectra obtained with the thick diaphragm are marked in Fig. 2 by red color, the areas under them are shown as gray-hatched regions, for clarity they are enlarged in the insets. Clear shoulder at channels 302 and 414, at the foot of a "big" peak at channels 650–660 measured with thin diaphragm, are seen in the spectra for samples H1 and ST, respectively (Fig. 2(a), (c)). In the spectrum for the H1 detector (Fig. 2(a)) the signals from higher energies are also present, that may indicate a nonuniformity of the film thickness, such as growth steps, or a global thickness gradient, in contrast to the ST sample with presumably a more uniform film. No shoulder in the alpha spectrum is seen for the sample H2, indicating the film thickness to be close to the stopping range for α-particles (13.6 μm). However, the thick-diaphragm spectrum of the H2 sample does not form a sharp peak but rather a broad distribution in 550–700 channel range. It means that some alphas penetrate through the CVD layer of the H2 sample, so the film thickness does not exceed 13.6 μm.

The thickness h of a diamond film (sensitive layer) can be determined from the position of the edge of the shoulder in the full α-spectra (non-collimated particles), or from position of the peak at almost perpendicular incidence of the well-collimated particles, selected with 8-mm thick diaphragm (further referred to as $\perp\alpha$-peak). In case of the α-particle passage through the film there is a certain scattering in the energy deposited within the film, that should be taken into account in its thickness estimate, therefore the following algorithm was used to determine the h value. First, the range of channels (ROI) was determined, where the $\perp\alpha$-peak is mostly located. The average channel number for the $\perp\alpha$-peak and root-mean square deviation were calculated within the ROI. The average peak position depends only slightly on the exact ROI limits. Assuming the α-peak maximum at $E_0 = 5.5$ MeV (and reduced by 15 keV due to the loss in the 100 nm-thick Al contact layer), the average energy $\langle E\rangle_{\mathrm{ROI}}$ deposited in the detector upon normal incidence was calculated. Next, the film thickness h was fitted with TRIM program (Monte-Carlo simulation in the SRIM software). In TRIM simulation both α energies of ^{238}Pu were taken into account (5.499 and 5.456 MeV) to calculate the average energy deposition in the active detector layer, fitted to $\langle E\rangle_{\mathrm{ROI}}$. For the particles passed through the ∅1.5 × 8 mm diaphragm the effective thickness is $h\langle\cos\theta\rangle = 0.99h$, where θ is the incidence angle. We took $\Delta h = \Delta E/S(E)$ as the error in the thickness, where ΔE is the energy root-meansquare deviation in the $\perp\alpha$-peak and $S(E) = dE/dx$ is the alpha stopping power in diamond, calculated for the α-particle energy $E = E_0 - \langle E\rangle_{\mathrm{ROI}}$ at the bottom of the detector layer. The results of the film thickness evaluation for the three samples, and the calculation parameters used, are given in Table 1. The

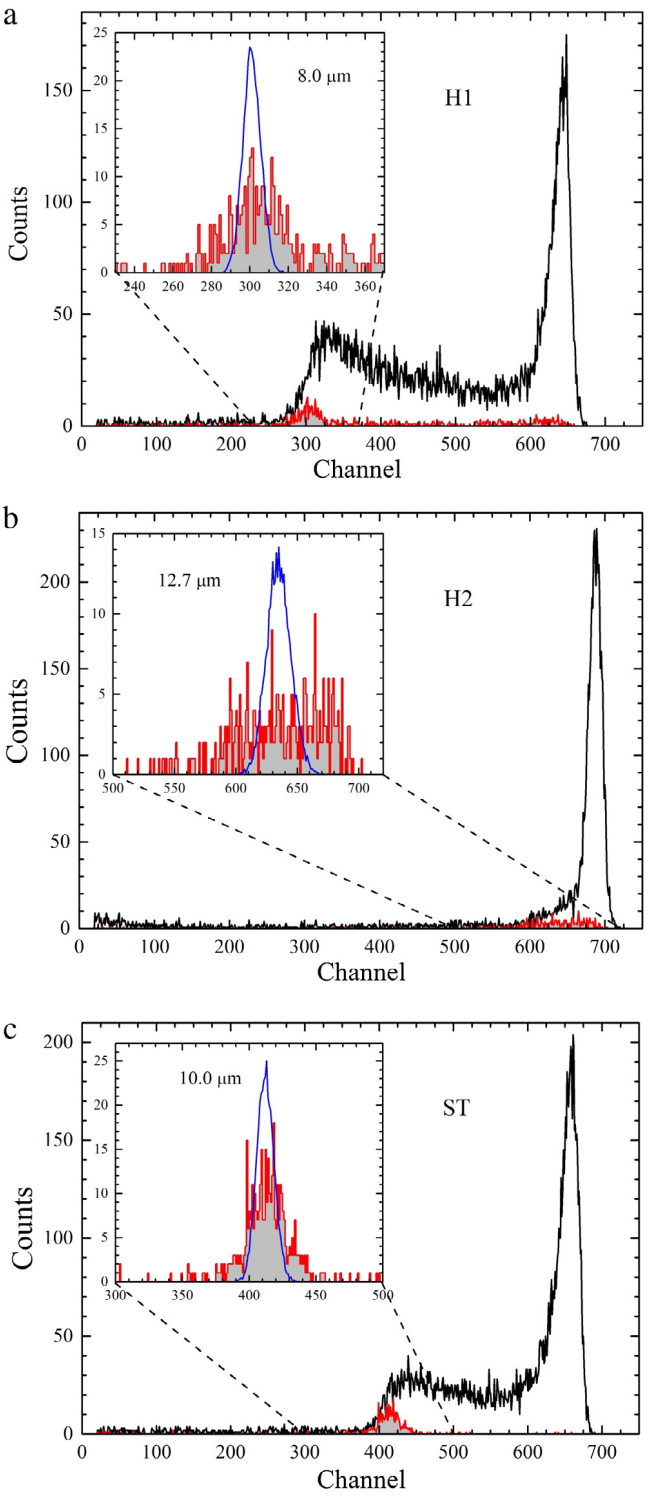

Fig. 2. The alpha spectra from ^{238}Pu source obtained with the detectors H1 (a), H2(b) and ST (c) taken with thin (1 mm) diaphragm (black spectra). The low-intensity red spectra are taken with thick (8 mm) diaphragm collimating the particle flux. Insets are zoomed spectra obtained with the thick diaphragm. The narrow blue profiles show TRIM simulation of the α-spectra with fitted diamond film thicknesses of 8.0, 12.7 and 10.0 μm, respectively. (For interpretation of the references to color in this figure legend, the reader is referred to the web version of this article.)

Table 1
Parameters of α-peak as measured with the thin diaphragm, and $\perp\alpha$-peak as measured for the particles collimated with 8 mm thick diaphragm, used to calculate of the diamond film thickness.

Detector #	H1	H2	ST
α-peak channel No.	648	689	661
α-peak width (FWHM), %	3.5	3.2	4.1
Channels range (ROI)	270–330	560–700	380–450
$\langle$Channel No. of $\perp\alpha$-peak$\rangle_{ROI}$	302 ± 13	639 ± 32	414 ± 14
$\langle E\rangle_{ROI}$, MeV	2.57 ± 0.11	5.10 ± 0.26	3.45 ± 0.11
Film thickness h, μm	8.0 ± 0.3	12.7 ± 0.4	10.0 ± 0.2

diamond film thicknesses of 8.0, 12.7 and 10.0 μm, were determined for the detectors H1, H2 and ST, respectively.

Insets in Fig. 2 show in more detail the $\perp\alpha$-spectra obtained with the thick diaphragm along with a calculated signal distribution (narrow blue profiles) for the thicknesses given in Table 1. The profiles of the deposited energy have been calculated with TRIM, taking into account the angular spread of incident alpha particles. For ST sample the fit profile matches very well to the measured spectrum (see inset in Fig. 2(c)), thus indicating a high thickness uniformity of the particular epitaxial film (this corroborates the observation, that the ST sample demonstrated the most flat surface, without a global curvature, according to our profilometry data).

3.2. Slow-neutron detection

The experiments on neutron irradiation were performed using ^{252}Cf isotopic source. One fission event produces 3.7 neutrons with Maxwellian energy distribution $E^{1/2}\exp(-E/1.57\ \text{MeV})$ [29], and about 8 γ-quanta with average energy of 0.9 MeV per one γ-photon [30]. The source was placed in the center of a cylindrical polyethylene neutron moderator of 140 mm radius and the wall thickness of 110 mm. It was found previously [18] that 22% of neutrons slow down to thermal velocities in this moderator, while γ-quanta pass it practically without any change in their spectrum.

The sample ST, having the largest area, was chosen for the test, it was placed in a screening metal case positioned in proximity to the moderator. The amplifier and multichannel analyzer were connected to the detector via a coaxial connector. The energy per channel ratio of 3.94 keV was determined from the ^{238}Pu α-peak position (to obtain a better resolution in lower signal range, the multichannel analyzer settings differed from those used to get spectra in Fig. 2). The lower threshold for signal discrimination was set at the channel 14, corresponding to energy 55 keV deposited in diamond.

The measurements were performed in two steps. First, the spectrum from ^{252}Cf was recorded without converter of slow neutrons. Then, a copper foil covered with 3 μm thick ^{10}B isotope was fixed in proximity of the detector surface, and the spectrum was measured again. After this, the foil was replaced with an adhesive tape with powder of lithium carbonate $^{6}Li_2CO_3$ enriched with ^{6}Li isotope. Each spectrum was recorded or 24 h. The measured spectra for the neutron source with and without converters are displayed in Fig. 3.

Without the converters, the major part of the spectrum is located within first 50 channels, corresponding to the deposited energy of less than 200 keV. The spectrum is a result of diamond interaction with Compton electrons knocked out from the diamond and housing material. With use of the converters the spectrum corresponds to γ-emission background in low energy channels, and the spectrum of the products of the converter's nuclei interaction with neutrons at higher energies. The γ-background in the spectra with ^{10}B converter exceeds that seen for ^{6}Li converter and for the case of without the converter. We attribute the enhanced background observed with the ^{10}B converter to the copper foil (having the high Z), which generated many Compton electrons under γ-irradiation.

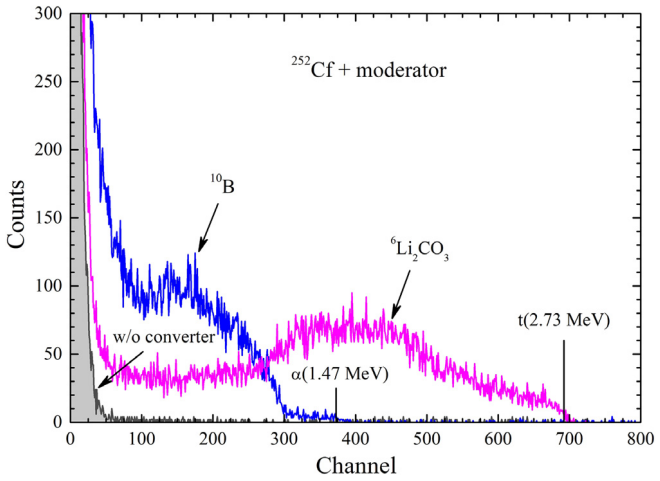

Fig. 3. The spectra from ST detector for the neutron source ^{252}Cf as measured with ^{10}B (blue spectrum) and $^{6}Li_2CO_3$ (violet spectrum) converters, and without the converter (black spectrum). The solid vertical lines show the maximum energy of nuclear fission products of the converter, as calculated from the position of α-peak for ^{238}Pu (channel 1395). The energy per channel is 3.94 keV. (For interpretation of the references to color in this figure legend, the reader is referred to the web version of this article.)

The right side of the spectrum is determined by the maximum energy of charged particles formed by the neutron-converter interactions [31]:

$$n + {}^{10}\text{B} \rightarrow \begin{cases} {}^{7}\text{Li}\,(1.01\ \text{MeV}) + \alpha\,(1.78\ \text{MeV}) & (6\%) \\ {}^{7}\text{Li}^{*}\,(0.84\ \text{MeV}) + \alpha\,(1.47\ \text{MeV}) & (94\%) \end{cases}$$

$$n + {}^{6}\text{Li} \rightarrow \alpha\,(2.05\ \text{MeV}) + t\,(2.73\ \text{MeV})\,.$$

A part of energy is dissipated upon slowdown of the particles within the converter, so the signal spectrum extends from zero to a maximum energy of the charged particles, if the reaction takes place near the top surface of the detector. The maximum energy of alpha particles is 1.47 MeV (with 94% probability) with ^{10}B converter, and 2.73 MeV for tritium in case of ^{6}Li converter. Those energies are shown at the high energy end of the spectra in Fig. 3, their positions are calculated from the energy/channel ratio. Thus, the signals from the converter-generated particles and the γ-background are effectively discriminated, especially using the ^{6}Li-containing converter.

3.3. Polarization effects

The results shown in Fig. 3 refer to a relatively weak laboratory neutron source, with the neutron flux of about 70 cm^{-2} s^{-1} [21]. The neutron count rates, after subtraction of the γ-background within 0–50 channels, was 0.25 and 0.31 s^{-1} for ^{10}B and $^{6}Li_2CO_3$ converters, respectively. This corresponds to about 3% of all neutrons, which hit detector in both cases. However, the detector response can change at high fluences due to a polarization, i.e. the accumulation of a charge in diamond bulk. We assessed the polarization effect by measuring α-spectra from ^{238}Pu source for a prolonged time, to obtain the doses up to 10^7 mm^{-2}. The evolution of the α-spectrum with irradiation time (10 min, 1 h and 5 h) for the detector ST is shown in Fig. 4(a) (here the amplifier and multichannel analyzer were different from those used for getting the data shown in Fig. 2, so exact α-peak positions are slightly different from the values in Table 1). The measurements were performed without the diaphragm, therefore, due to the edge effect, the spectra revealed a small difference from that shown in Fig. 2(c). It is seen that the α-peak decreases and shifts to lower energies with the α exposure time, indicating a reduction in charge collection efficiency.

As the detectors H1 and H2 revealed much lower polarization rate compared to the sample ST, we used for their tests a more powerful ^{238}Pu isotope source with the intensity of 7 times higher than that for the ST

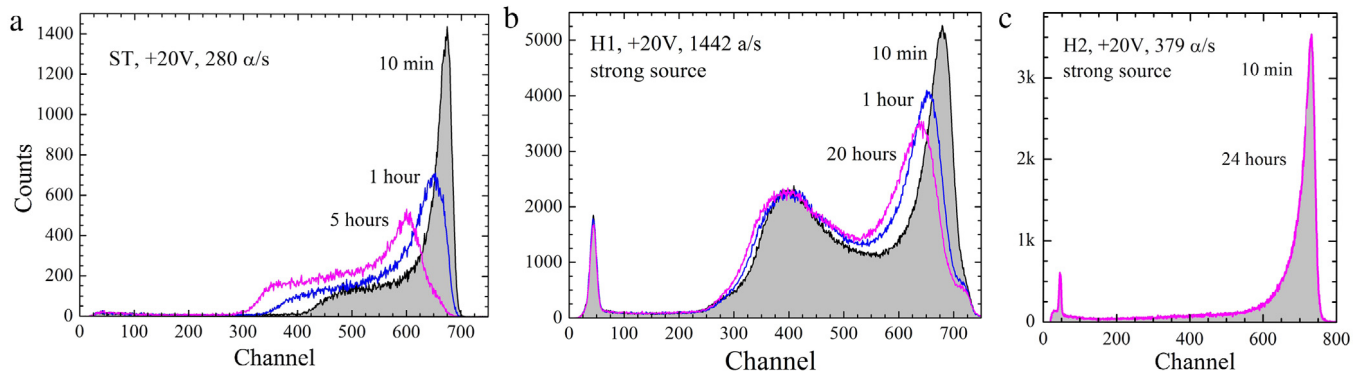

Fig. 4. The evolution of the α-spectrum ^{238}Pu with irradiation time for the samples ST (a), H1 (b) and H2 (c). A higher flux ^{238}Pu source was used for H1 and H2 detector test. Note the signal degradation with exposure time due to polarization effect for the samples ST and H1.

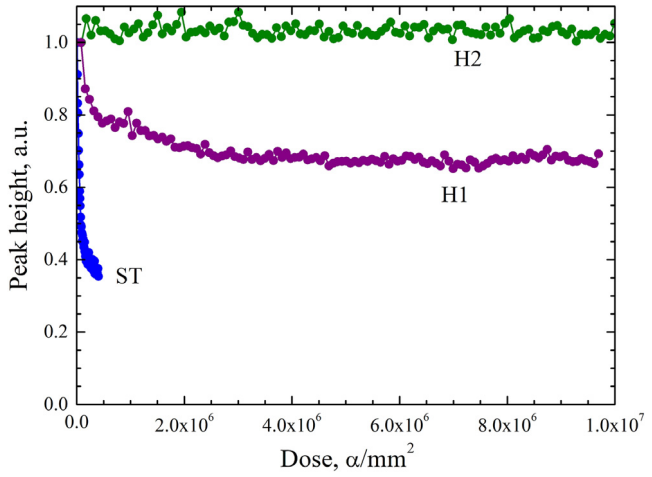

Fig. 5. Dose dependences of the α-peak height at the ^{238}Pu-source irradiation for the samples H1, H2 and ST (the peak heights are normalized to unity at the beginning of irradiation). The bias voltage is +20 V.

device. The signal evolution with time for the sample H1 is shown in Fig. 4(b). The alpha peak decreases in a few hours and then stabilizes, the difference between 1 and 20 h spectra is rather small. For the most stable detector H2 no change in the spectrum was observed for 24 h exposure as shown in Fig. 4(c).

The results on polarization effect for the three samples are summarized in Fig. 5. The plots are given for the normalized α-peak intensity vs dose of 5.5 MeV alphas as measured at +20 V bias voltage (the field $E = 2$ V/μm). The dose was calculated for the area of the top *Al* contact only, neglecting the naked edge zone. The α-peak height for ST sample reduced by two times after the dose of 10^5 mm^2, the sample H1 response stabilizes after the dose of 5×10^6 mm^2, while no polarization is seen for H2 sample up to dose of 10^7 mm^2. After bias was switched off for 1 min and then switched on again, the initial spectrum was completely restored for each of the detectors. We note, that prior the polarization test, the ST sample received quite low dose upon neutron exposure, when the data for Fig. 3 were collected, but those doses were too low to cause enough radiation damage supporting the observed polarization effect at that stage. Therefore, we attribute the observed enhanced polarization for ST exclusively to its more intrinsic defected structure, rather than to accumulation of radiation defects before the polarization kinetics test.

As the sample preparation procedure (growth, ion implantation, annealing) was nominally identical for all the three specimens, the difference in the polarization effect between them can be ascribed to a difference in abundance of growth defects, such as dislocations, originated from the film/substrate interface [32]. The substrates in the present study were of different origin, with presumably different (uncontrolled) dislocation density and defect contents. The dislocations and other point and extended defects can serve as long-lived traps, charged during the irradiation process. As established in [20] by the Transient Current Technique for a 0.5-mm thick single crystal diamond detector, the charged traps induce a build-in electric field compensating the bias field, thereby reducing the charge collection efficiency. When bias is switched off but the source is not removed, the build-in field induces the current in reverse direction, which discharges the traps and restores detector to its initial state. We note that although the He^+ ion implantation does induce defects, they are not responsible for the polarization observed since the H2 sample shows no spectrum degradation.

4. Conclusions

We fabricated thin epitaxial diamond film detectors, with a buried graphite electrode layer 8–12 μm deep produced by He^+ ion implantation and annealing. The energy spectra for 5.5 eV alpha particles were obtained with α-peak width (FWHM) of 3.6 ± 0.4%. The alpha spectrum features were used to estimate the film thickness with accuracy of better than 0.4 μm. Using ^{10}B and ^{6}Li isotopes as converters, which produce charge particles with maximum energy of 1.47 MeV and 2.73 MeV, respectively, the thin film sensors were tested for detection of neutron and γ-radiation from ^{252}Cf source. By comparing the detector signals with and without the converter it was possible to discriminate the contribution of γ-quanta in the spectrum from that of the neutron related signal. We showed that the small thickness of sensitive diamond layer allows a strong reduction of the γ-background impact on the detector response. The best quality detector demonstrated high stability under exposure to α-particles from ^{238}Pu isotope source, with no sign of polarization at least up to dose of 10^7 mm^{-2} at flux of 130 mm^{-2} s^{-1}. Another advantage of the reported device is its capability to work with low bias (20 V in our case). Also, the use of thin diamond film detectors is expected to significantly increase the detector radiation hardness compared to common ~0.5 mm thick diamond plates [8]. Moreover, high energy resolution can be achieved with thin diamond single crystal neutron detectors, as demonstrated recently by Shimaoka et al. [9] for a 70 μm thick free-standing film separated from the substrate by lift-off technique. In view of these benefits the use of different versions of thin film detectors for neutrons and other high energy particles deserves a further attention.

Acknowledgments

The authors are thankful to E.V. Zavedeev for the sample profilometry work. A.P.B and V.G.R. acknowledge the support from International Science & Technology Cooperation Program of China (2015DFR50300) and 1000 Talents Program.

References

[1] M. Marinelli, E. Milani, G. Prestopino, A. Tucciarone, C. Verona, G. Verona-Rinati, M. Angelone, D. Lattanzi, M. Pillon, R. Rosa, E. Santoro, Appl. Phys. Lett. 90 (2007) 183509.

[2] P. Lardon, C. Mer, P. Delacour, B. Bazin, D. Tromson, S. Normand, M. Nesladek, F. Foulon, P. Bergonzo, Diam. Relat. Mater. 15 (2006) 815–821.

[3] S. Almaviva, M. Marinelli, E. Milani, G. Prestopino, A. Tucciarone, C. Verona, G. Verona-Rinati, M. Angelone, M. Pillon, Nucl. Instrum. Methods Phys. Res. A 612 (2010) 580–582.

[4] M. Angelone, D. Lattanzi, M. Pillon, M. Marinelli, E. Milani, A. Tucciarone, G. Verona-Rinati, S. Popovichev, R.M. Montereali, M.A. Vincenti, A. Murari, JET-EFDA Contributors, Nucl. Instrum. Meth. Phys. Res. A 595 (2008) 616–622.

[5] S. Almaviva, M. Marinelli, E. Milani, G. Prestopino, A. Tucciarone, C. Verona, G. Verona-Rinati, M. Angelone, D. Lattanzi, M. Pillon, R.M. Montereali, M.A. Vincenti, J. Appl. Phys. 103 (2008) 054501.

[6] J.H. Kaneko, T. Teraji, Y. Hirai, M. Shiraishi, S. Kawamura, S. Yoshizaki, T. Ito, K. Ochiai, T. Nishitani, T. Sawamura, Rev. Sci. Instrum. 75 (2004) 3581–3584.

[7] M. Marinelli, E. Milani, G. Prestopino, M. Scoccia, A. Tucciarone, G. Verona-Rinati, M. Angelone, M. Pillon, D. Lattanzi, Appl. Phys. Lett. 89 (2006) 143509.

[8] M. Osipenko, M. Ripani, G. Ricco, B. Caiffi, F. Pompili, M. Pillon, G. Verona-Rinati, R. Cardarelli, Nucl, Instrum. Methods Phys. Res. A 817 (2016) 19–25.

[9] T. Shimaoka, J.H. Kaneko, K. Ochiai, M. Tsubota, H. Shimmyo, A. Chayahara, H. Umezawa, H. Watanabe, S. Shikata, M. Isobe, M. Osakabe, Rev. Sci. Instrum. 87 (2016) 023503.

[10] D. Lattanzi, M. Angelone, M. Pillon, S. Almaviva, M. Marinelli, E. Milani, G. Prestopino, A. Tucciarone, C. Verona, G. Verona-Rinati, S. Popovichev, R.M. Montereali, M.A. Vincenti, A. Murari, Fusion Eng. Des. 84 (2009) 1156–1159.

[11] V.N. Amosov, S.A. Meshaninov, N.B. Rodionov, R.N. Rodionov, Diam. Relat. Mater. 20 (2011) 1239–1242.

[12] M. Pillon, M. Angelone, A. Krása, A.J.M. Plompen, P. Schillebeeckx, M.L. Sergi, Nucl. Instrum. Methods Phys. Res. A 640 (2011) 185–191.

[13] A.V. Krasilnikov, J. Kaneko, M. Isobe, F. Maekawa, T. Nishitani, Rev. Sci. Instrum. 68 (1997) 1720–1724.

[14] B. Bentele, J.P. Cumalat, D. Schaeffer, S.R. Wagner, G. Riley, S. Spanier, Nucl. Instrum. Methods Phys. Res. A 838 (2016) 74–81.

[15] A. Kumar, A. Kumar, A. Topkar, D. Das, Nucl. Instrum. Methods Phys. Res. A 858 (2017) 12–17.

[16] F. Gagnon-Moisan, A. Zimbal, R. Nolte, M. Reginatto, H. Schuhmacher, Rev. Sci. Instrum. 83 (2012) 10D906.

[17] M. Pillon, M. Angelone, G. Aielli, S. Almaviva, M. Marinelli, E. Milani, G. Prestopino, A. Tucciarone, C. Verona, G. Verona-Rinati, J. Appl. Phys. 104 (2008) 054513.

[18] K. Zyablyuk, V. Kolyubin, V. Pashentsev, P. Nedosekin, E. Tyurin, M. Afanas'ev, Inorg. Mater. 52 (2016) 262–267.

[19] N.B. Rodionov, V.N. Amosov, K.K. Artem'ev, S.A. Meshchaninov, V.P. Rodionova, R.A. Khmel'nitskii, V.A. Dravin, A.P. Bol'shakov, V.G. Ral'chenko, At. Energy 121 (2016) 126–134.

[20] M. Rebai, A. Fazzi, C. Cazzaniga, G. Croci, M. Tardocchi, E. Perelli. Cippo, C.D. Frost, D. Zaccagnino, V. Varoli, G. Gorini, Diam. Relat. Mater. 61 (2016) 1–6.

[21] S.A. Afanas'ev, A.P. Bol'shakov, V.A. Dravin, K.N. Zyablyuk, V.A. Kolyubin, P.G. Nedosekin, V.N. Pashentsev, V.G. Ral'chenko, E.M. Tyurin, R.A. Khmel'nitskii, Russ. Eng. Res. 37 (2017) 354–358.

[22] The Stopping and Range of Ions in Matter. http://www.srim.org.

[23] New Diamond Technology, http://ndtcompany.com/.

[24] Soni Tools, http://www.sonitools.com/.

[25] A.P. Bolshakov, V.G. Ralchenko, V.Y. Yurov, A.F. Popovich, I.A. Antonova, A.V. Khomich, I.I. Vlasov, E.E. Ashkinazi, S.G. Ryzhkov, A.V. Vlasov, A.A. Khomich, Diam. Relat. Mater. 62 (2016) 49–57.

[26] A.V. Khomich, R.A. Khmelnitskiy, V.A. Dravin, A.A. Gippius, E.V. Zavedeev, I.I. Vlasov, Phys. Solid State 49 (2007) 1661–1665.

[27] A.A. Gippius, R.A. Khmelnitsky, V.A. Dravin, A.V. Khomich, Defect-induced graphitisation in diamond implanted with light ions, Physica B 308 (2001) 573–576.

[28] G. Bachingjagian, D. Karmanov, E. Kouznetsov, M. Merkin, A. Savin, A. Voronin, Design and features of an electronics engineering of a detection part the Hadron-Electron Separator of experiment ZEUS (DESY), Preprint NPI MSU 2000-3/607.

[29] J.W. Meadows, Phys. Rev. 157 (1967) 1076–1082.

[30] V.V. Verbinski, H. Weber, R.E. Sund, Phys. Rev. C 7 (1973) 1173–1185.

[31] Evaluated Nuclear Data File (ENDF), National Nuclear Data Center, Brookheaven National Laboratory, http://www.nndc.bnl.gov/.

[32] A. Tallaire, T. Ouisse, A. Lantreibecq, R. Cours, M. Legros, H. Bensalah, J. Barjon, V. Mille, O. Brinza, J. Achard, Cryst. Growth Des. 16 (2016) 2741–2746.